PAPER

Electronic properties of a pristine and NH$_3$/NO$_2$ adsorbed buckled arsenene monolayer

Md. Shahzad Khan,[a] Anurag Srivastava[*a] and Ravindra Pandey[b]

Analogous to exfoliated 2D sheets of black phosphorene, arsenene is an atomically thin layer of the arsenic crystal. In this paper, we investigate the sensitivity of a pristine arsenene sheet for NH$_3$ and NO$_2$ molecules in terms of binding energy, nature of bonding, density of states and current–voltage characteristics. The calculated results based on density functional theory find that both NH$_3$ and NO$_2$ molecules show a significant affinity for arsenene leading to strong physisorption with significant electronic charge transfer. The calculated I–V characteristics reveal that physisorption of NH$_3$ and NO$_2$ induces modifications in the conductivity of pristine arsenene. Incorporation of Ge in arsenene leads to enhanced binding of NH$_3$ and NO$_2$ *via* chemisorption on arsenene.

1 Introduction

In the last few years great attention has been paid to atomically thin layers of group V elements. In this quest, researchers have studied phosphorene (obtained from phosphorus) more extensively.[1–3] Recently, the experimental existence of black phosphorene and theoretical prediction of blue phosphorene have been confirmed. Subsequently this single layered novel nanostructure further fascinated researchers to look for other possible quasi 2D-nanosheets of group V-elements. In this race, analogous to exfoliated 2D nanosheets of silicene, germenene, phosphorene, arsenene, antimonene and stanane are proposed. Although graphene is not found to be an effective adsorbent for small organic molecules like ammonia, acetone, acetonitrile, benzene, methane, methanol, ethanol, and toluene. Comparatively these rippled surfaces of silicene and germenene are good adsorbent.[4,5] Silicene and germenene is zero band semiconductor and adsorption of such organic molecule generally introduced opening of band gap. Several works suggest that these quasi 2D materials show quantum spin Hall effect (QSH) transistor behaviour on functionalization, followed by straining.[6–8] Such QSH two dimensional topology play important role in spintronic devices. The structural and electronic properties of arsenene and antimonene (from antimony) have been characterized[9–11] using first principles methods. Kamal *et al.*[9] claimed for the arsenene in puckered phase as stable configuration compare to buckle one. Their phonon calculations for buckled arsenene resulted imaginary frequency near Γ point for transverse acoustic mode, and anticipated it as reason of some

computational disparity. Contrary to this Zhang *et al.*[10] have reported a stable buckled phase with no imaginary frequency found in phonon calculation. These research efforts although addresses well the structural and electronic characterization but didn't discuss its any applications. On other hand in the last few years, efforts have been made to look at the better 1D or 2D nanomaterial for sensing the toxic gases/chemicals in its surroundings. Hence, we thought it is pertinent to explore the possibility of arsenene as relatively better sensing material than existing carbon allotropes for molecules of ammonia (NH$_3$), and nitrogen dioxide (NO$_2$). It is well established fact that NH$_3$ and NO$_2$ are products of various chemical and biological processes and are considered to be hazardous. For example, NH$_3$ is generally found in common industrial environment and NO$_2$ is primarily emitted by motor vehicles. NO$_2$ is also precursor for a number of harmful secondary air pollutants like nitric acid, aerosols and photo oxidants. Previously, sensing characteristics of the well-known 1D and 2D carbon allotropes, through adsorption analysis have been extensively reported by our group[12–19] as well as by others.[20–24] In present work we intentionally examine the buckled phase arsenene for NH$_3$ and NO$_2$ molecule. We also investigate the possibility of the arsenene-based devices for applications in sensing of toxic gases.

First ground state calculations under self-consistent field are performed to obtain minima at potential energy surface for pristine buckled arsenene sheet. Subsequently, analysis of structural parameter and electronic properties like phonon spectra, natural bond orbital (NBO),[25] density of state (DOS), bandstructure, highest occupied molecular orbital (HOMO) and the lowest unoccupied molecular orbital (LUMO) are scrutinized. To check the convergence of employed theory for present work, structural and electronic characterization and its comparison with other findings[9,10] have been reported at the initial stage of work. The sensitivity of arsenene towards NH$_3$

ª Advanced Materials Research Group, CNT Lab, ABV-Indian Institute of Information Technology and Management, Gwalior, M. P. 474015, India. E-mail: profanurag@gmail.com

ᵇ Department of Physics, Michigan Technological University, Houghton, USA

and NO$_2$ molecules has been analyzed in terms of binding energy, charge transfer, DOS, charge decomposition analysis (CDA) and current–voltage characteristic (*I–V*). We also consider the case of Ge-doped arsenene to determine the relationship between the affinity of molecules and dopant in the 2d lattice.

2   Computational method

Electronic calculations have been performed in the framework of density functional theory (DFT) using Gaussian09 (G09).[26] Additionally, we employed the Atomistix-tool-kit Virtual nano-lab (ATK-VNL) program package[27] to investigate properties of arsenene-based device consisting of a quasi 2D-sheet. Fig. 1 display the optimized cluster and periodic buckled arsenene: a finite cluster model for G09 calculations and a periodic supercell model for ATK-VNL calculations are considered. The cluster model consists of 54 As-atoms with hydrogen passivation at edge atoms. In G09 calculations, the generalized exchange correlation in terms of Perdrew–Burke–Ernzherof (PBE)[28] type parameterization along with the 6-31g(d) basis sets are used. Frequency calculations are performed to ascertain the ground state configuration of the system. DOS and CDA calculations have been performed using G09 output within AOMix[29–35] software package. For ATK calculations, the PBE-DFT approximation along with the double-ζ-polarized (DZP) basis set and Troullier–Martins[36] pseudo-potentials are considered. Split-valence double-ζ-polarized basis set are sufficient for computational convergence. The norm-conserving Troullier–Martins pseudo-potential describes the interaction between ionic cores and localized pseudo-atomic orbitals. A (14.4 Å × 14.4 Å × 15 Å) supercell having 32 As atoms is chosen. The

distances between periodic images of arsenene are kept at 15 Å to avoid interlayer interaction. The sampling of reciprocal space with (8 × 8 × 1) *k*-points is made using Monkhorst–Pack scheme[37] for geometry optimization, while *k*-point sampling are set at 16 × 16 × 1 for calculations of electronic properties. For odd electronic configuration of NO$_2$-arsenene sheet, spin-polarized calculations have been performed. The combination of DFT and Non-Equilibrium Green's Function (NEGF) method[38] in ATK-VNL is made to derive electron transport calculations. This calculation is important for finding transmission spectra at different bias windows its derivative current–voltage (*I–V*) characteristics.

3   Results and discussion

3.1   Pristine arsenene

The stability of buckled arsenene has been confirmed through phonon calculations and thus validates the employed theoretical approach for further investigations. No imaginary frequencies were found. Likewise, Fig. 2 shows no soft modes confirming the stability of arsenene. Additionally, the convergence of geometrical parameters for arsenene from the cluster (G09) and the periodic supercell (ATK) approaches signify the appropriateness of these approaches in our work. For example, the calculated As–As bond length is 2.45 Å from G09 and is 2.5 Å from ATK. The calculated bond angle between adjacent atoms (<As–As–As) are 90.5° and 91° obtained from G09 and ATK, respectively. Table 1 lists the measured bond-length and bond-angles of arsenene along with the calculated values from previous reports. The calculated band structure, shown in Fig. 3, exhibits an indirect band gap of 1.83 eV which lies in-
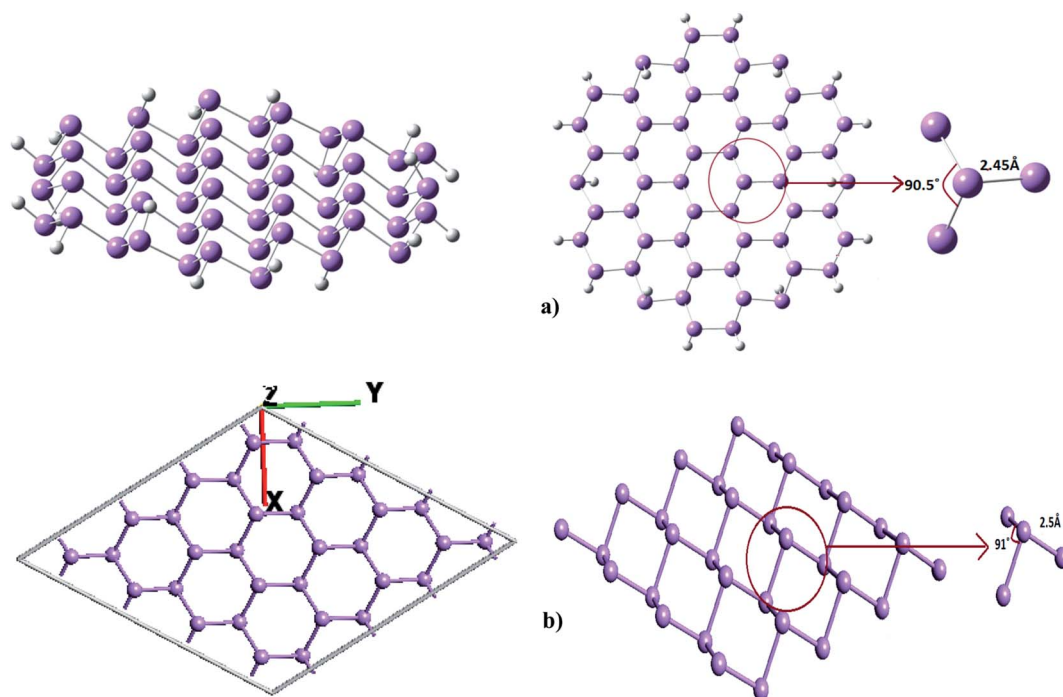

Fig. 1   (a) Finite cluster and (b) periodic supercell representing single layer arsenene sheet.
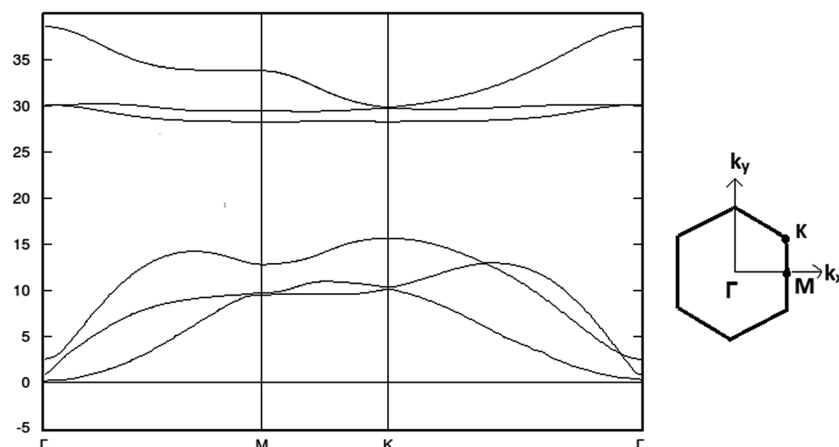
Fig. 2 Calculated phonon dispersion curves along high symmetry direction in the periodic supercell model.

between the calculated values of 1.635 eV (ref. 9) and 2.28 eV.[10] From the device point of view to exploit the buckled arsenene as conducting channels, it must have high electron mobility which is inversely proportional to its effective mass.[39] The effective mass of electron (m_e) is calculated to be $0.18m_0$ and $0.52m_0$ for Γ–K and Γ–M directions, respectively, assuring high mobility of electrons along these particular directions.

Similar to blue phosphorene, atoms in arsenene have sp^3 character at lattice point. The NBO analysis reveals that the lone pair electrons are mainly localized on 4s-subshell and the 4p electrons are engaged in the σ-bonding formation. The inter-frontier orbital analysis confirms that HOMO is delocalized with contributions from σ- and lone pair electronic density (Fig. 4a). On the other hand, localized LUMO is primarily σ* in nature (Fig. 4b) for arsenene. From molecular orbital diagram it is clear that electronic charge is mainly localized on atomic center which make arsenene different from graphene. In graphene C-atoms are present at vertex of two dimensional honey comb lattice structure, this planarity enhance conjugation in between adjacent bond and results in delocalization of electronic density. Contrary, in the arsenene lattice As atoms are in two different planes (up and own), in each ring which inhibit such conjugation effects.

3.2 NH₃ and NO₂ adsorbed arsenene

To investigate the NH_3 and NO_2 adsorption on arsenene, several possible adsorption sites including top of the each atoms, centre of As–As bond and centre of the hexagonal ring have been

considered. Fig. 5(i), depict different orientation of NH_3/NO_2 considered over arsenene sheet before optimization at reasonable distance. For present context, NH_3 and NO_2 affinity towards arsenene surface is analysed in terms of adsorbate (NH_3/NO_2) and adsorbent interaction *i.e.*, adsorption. The phenomenon of adsorption plays an important role in understanding sensitivity of surface towards exotic molecules. If adsorption is strong *i.e.* by means of charge transfer interaction this may be label as chemisorption. Comparatively physisorption has nothing to do with charge transfer mechanism and interaction between adsorbate and adsorbent is *via* van der Waals forces. Typically interaction energy in this case lies in-between 0.01 eV to 0.1 eV.[40] For NH_3, the ground state calculation reveals N pointing to arsenene surface with hydrogen atoms on next end as preferred orientation of the molecule. Likewise, N at the centre of symmetrical O–N–O bond actively participates with arsenene. The preferred site for NH_3 was found to be centre of ring as shown in Fig. 5 with the adsorption energy of 0.87 eV. Here, N atom was symmetrically away from upper layer arsenene atom with the bond distance of 3.01 Å. In contrary, Wang *et al.*[4] reported NH_3 is comparatively less bonded with germenene having binding energy of −0.459 eV with N pointing towards one of Ge atom. Both NBO analysis and molecular orbital density contour plots suggested noticeable interaction between NH_3 and arsenene. The lone pair orbital at N of NH_3, donates a partial charge of about $0.11e$ to arsenene, thus NH_3 brings changes in electronic density of the inter-frontier orbitals associated to arsenene sheet. The HOMO–LUMO gap is now reduced to 2.4 eV for the arsenene sheet. NO_2 adsorbed configuration of arsenene exhibits lowering of inter-frontier orbital to 2.23 eV for spin-up states and 0.79 eV for spin-down states. This change in orbital energy levels can be seen as intimacy of arsenene towards NO_2. The contour plots at $0.04e$ per Å^3 shown in Fig. 5 depict overlapping of the empty valence p-orbital of N from NO_2 with non-bonding lone pair orbitals of arsenene. This overlapping is missing for NH_3 molecules in present contour context. The reason could be inter-electronic repulsion between NH_3 and arsenene lone pair electronic cloud. The calculated PDOS (Fig. 6) verify these

Table 1 Geometrical parameters of optimized arsenene through G09 and ATK package along with earlier reports

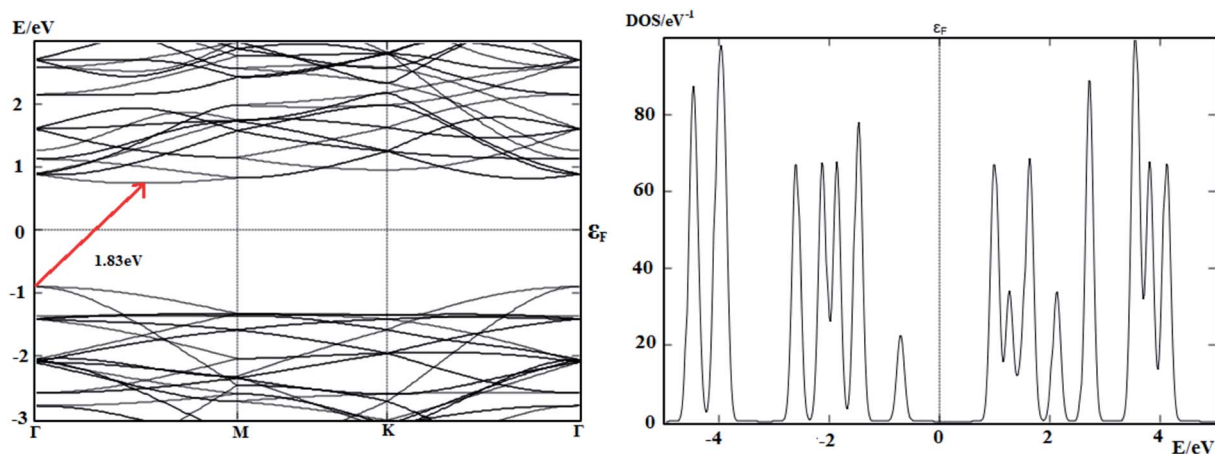| Geometrical parameters	G09	ATK	Earlier findings
Bond-length (As–As)	2.45 Å	2.5 Å	2.50 Å (ref. 4), 2.45 Å (ref. 5)
Bond angle (<As–As–As)	90.5°	91°	92.2° (ref. 4), 92.5° (ref. 5)

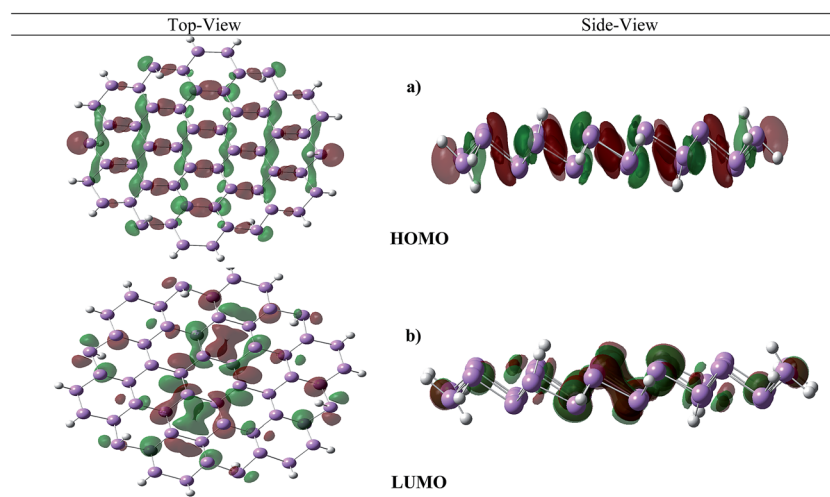Fig. 3   Calculated band structure and DOS of arsenene in the periodic supercell model.

Fig. 4   Electronic charge density associated with the inter-frontier orbitals of arsenene.

contour plots in concern of N-valence p orbital from NH_3, NO_2 and geometrically closed As from arsenene. The active participation of these fragments at inter-frontier orbital sites could be observed.

The ATK calculated electronic properties also show resemblance to the G09 calculated electronic properties suggesting a convergence of finite cluster and periodic supercell approach for present arsenene model. Note that both finite cluster and periodic supercell approaches find a feeble affinity of NH_3 and NO_2 towards arsenene.

3.3   Charge decomposition analysis

To get a detailed insight into bonding characteristics of the adsorbed arsenene system, we now perform charge decomposition analysis of the system. The fragmentation of adsorbate (second fragment orbital (2nd FO)) and adsorbent (first fragment orbital (1st FO)) of adsorbate + adsorbent (whole) and further derivation of wave functions for the whole from 1st and 2nd FO as their linear combination[35] calculated in CDA

analysis.[41,42] kth molecular orbital Ψ_k of whole system represented as,

$$\psi_k = \sum_k \sum_i c_{ik} \Phi_{i,k} \tag{1}$$

$\Phi_{i,k}$ is ith fragment orbital of kth fragments with $k = 1, 2$ and c_{ik} is fragment orbital coefficients. For the NH_3 adsorbed arsenene, the CDA analysis suggests the presence of a charge interaction which is mainly governed by mixing of occupied molecular orbital of one fragment with unoccupied of other. This computes the mode of interaction is *via* strong physisorption, where small self-polarizations of fragments in presence of each other have insignificant contribution. Similarly, a close inspection by performing CDA on NO_2 adsorbed arsenene finds spin-up states with $0.06e$ charge transfer from NO_2 to arsenene. This is not the case with spin-down states where NO_2 gains $0.16e$ from arsenene, resulting in total charge transfer of $0.95e$ between sheet and NO_2. Since self polarization for spin-up states are more prominent compare to spin-down states, the mode of adsorption appears to be a strong
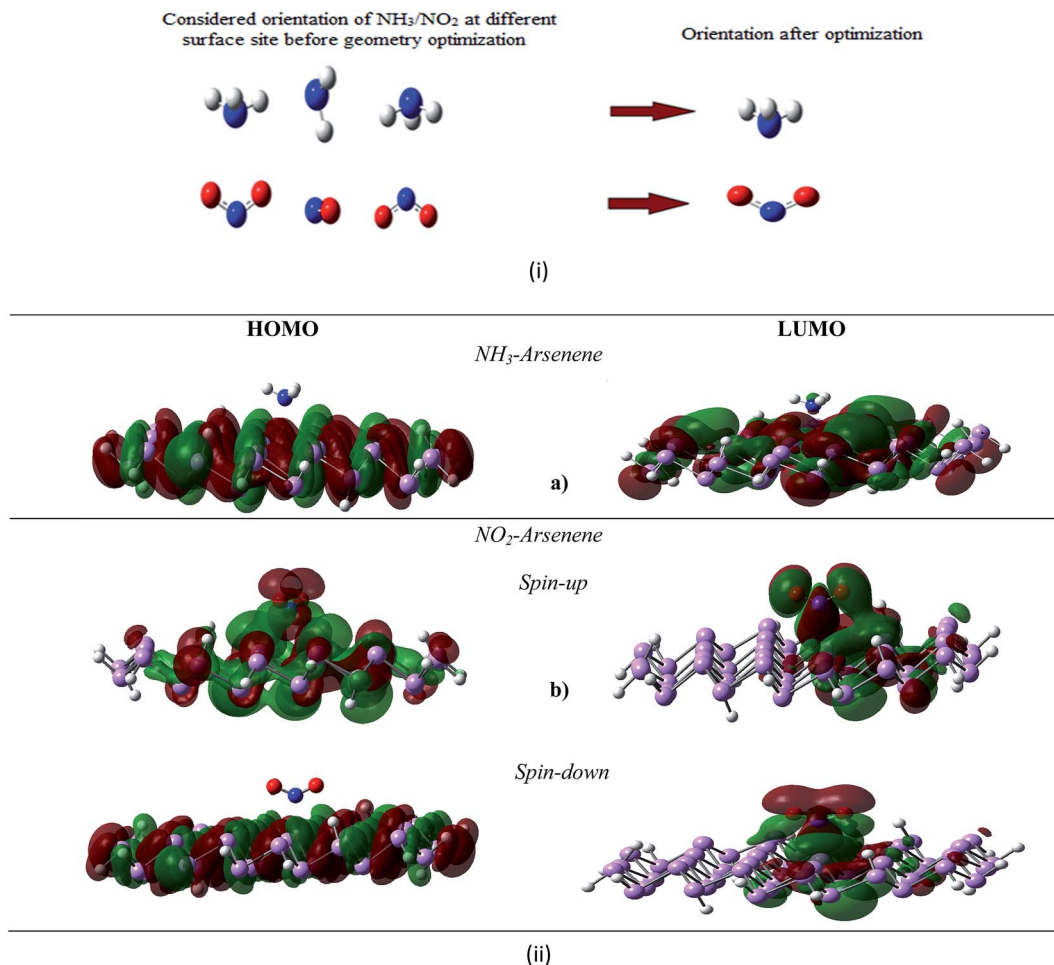
Fig. 5   (i) Different NH₃/NO₂ orientation considered towards arsenene sheet and (ii) electronic charge density associated with the inter-frontier orbitals of (a) NH$_3$-arsenene and (b) NO$_2$-arsenene.

physisorption or quasi chemisorption of gas molecules on arsenene.

3.4   Arsenene-based device: current–voltage characteristics

The above discussion is mainly focused on electronic analysis for NH$_3$ and NO$_2$ affinity for arsenene surface. These adsorption induced charge transformation should lead to the conductivity variation of the adsorbent. To investigate such variation in conductivity, the NEGF method has been employed to compute the transmission spectra at different bias voltage across the arsenene in two probe device models. Subsequently, the current–voltage characteristics are drawn from the calculated transmission coefficients.

The transmission function of a system is sum of transmission probabilities of all channels that particularly being results due to external bias (V), represented as

$$T(E, V) = T_r[\Gamma_L(E, V)G^R(E, V)\Gamma_R(E, V)G^A(E, V)] \qquad (2)$$

$G^{R/A}$ is retarded and advanced Green's functions and coupling functions $\Gamma_{L/R}$ represent imaginary part of left and right self energies, respectively. This expression is further introduced to Landuer–Bittier Formula[43] to evaluate the current as integration of the transmission function over the bias window near the Fermi level:

$$I = \frac{2e}{h} \int_{\mu_2}^{\mu_1} T(E, V) \Big[f(E - \mu_1) - f(E - \mu_2) \Big] \mathrm{d}E \qquad (3)$$

$f(E - \mu_{1/2})$ is Fermi distributions functions of electrons in left or right electrodes and $\mu_{1/2}$ are chemical potentials of left and tight electrodes.

Although the model arsenene possess structural anisotropy, in our analysis we have considered orthogonal in plane direction to armchair one, i.e. edged As-atoms on arsenene sheet have zig–zag arrangement along the length of model device. Two-probe models were used with semi-infinite left and right electrode regions in contact with the central region shown in Fig. 7. The length of each electrode and the central scattering region is ≈14 A along z-axis. Application of the external field to electrodes results in shifting of Fermi level. Matching of the valance band maxima of left electrode with the conduction band minima of right electrode generally leads to flow of current in the device.
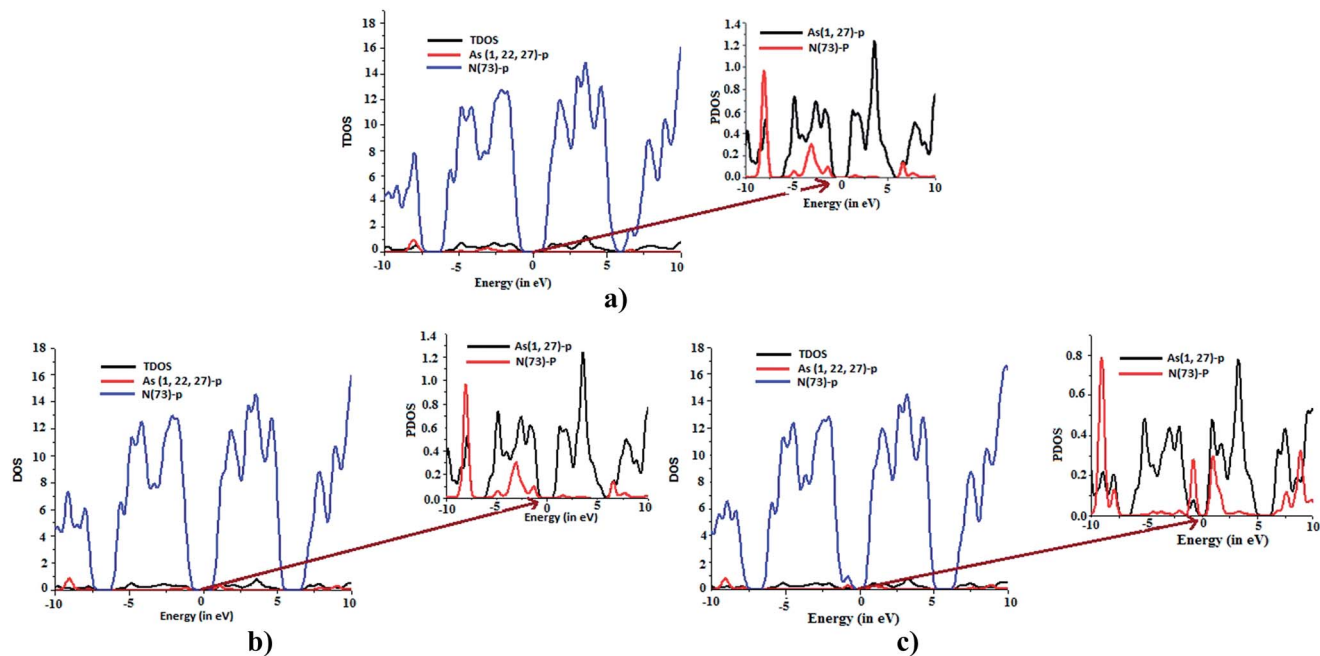
Fig. 6 Calculated DOS for adsorbate and adsorbent (a)NH$_3$-arsenene, (b) and (c) for up and down spin states for polarized NO$_2$-arsenene calculations, respectively.

Fig. 8 and 9 show the transmission spectra of pristine arsenene derived current at different bias voltage up to 8 V, respectively. There is a negative differential resistance (NDR) region found for all three cases suggesting this as signature of the pristine arsenene. To cross check any numerical convergence artefact that might consequence to NDR, negative biases were also applied across the electrode in the pristine arsenene device model, which completely rule out our perception. For the pristine arsenene, the *I–V* curve (Fig. 9) suggests that there is no current till 4.8 V. This threshold value of the applied bias is larger than the calculated bandgap of 1.73 V and can be seen for elucidation of high localized electronic charge in the 2d lattice. After the bias of 4.8 V, a significant current flows through the device rising upto 12.3 nA at 6 V. However beyond this bias voltage, the negative resistance behaviour of arsenene device model is exhibited till 6.7 V. Further rise in applied bias yields
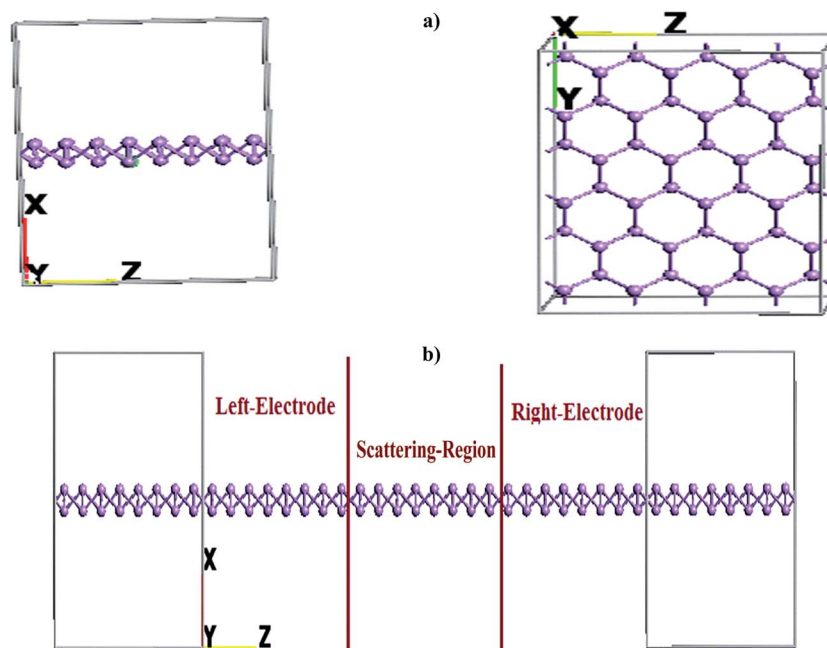

Fig. 7 Schematic of two probe device model for arsenene. (a) Electrode and (b) device consisting of electrodes and scattering regions.
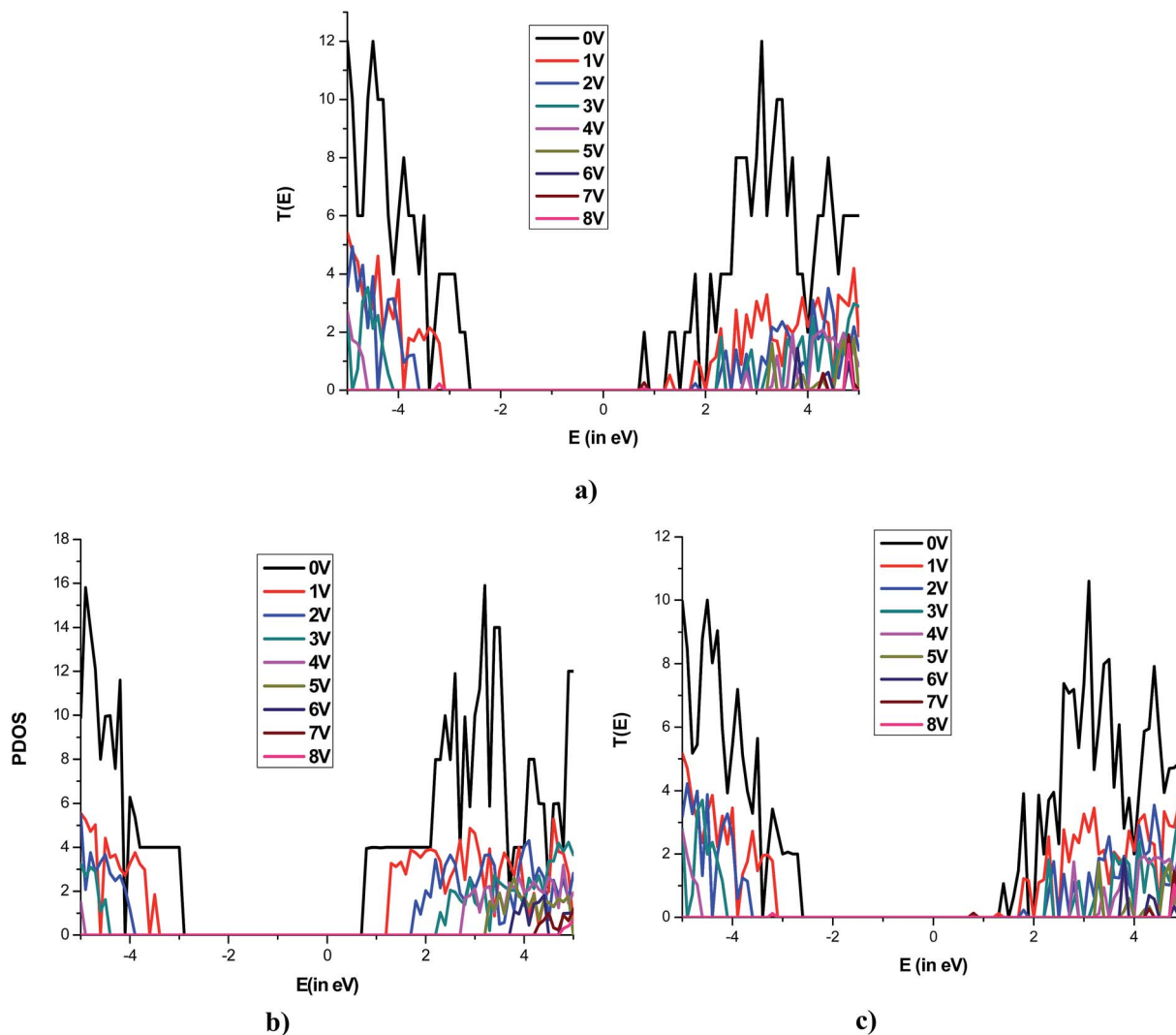
Fig. 8 Transmission spectra at different applied bias voltage for (a) arsenene, (b) NH$_3$-arsenene and (c) NO$_2$-arsenene.

into a nonlinear behaviour of the current–voltage characteristics. The presence of NH$_3$ molecule results in increased resistivity of arsenene sheet by inhibiting conduction channel across the Fermi level as is evident from Fig. 8b. At applied voltage of about 7.2 V, significant current begin to observe and afterwards the current voltage relation follow Ohmic behaviour in NH$_3$ sense arsenene model. Compare to NH$_3$, NO$_2$ presence on arsenene relatively increased conductivity but for the same transmission spectra plotted as Fig. 8c doesn't convey any information. It is expected that withdrawing nature of NO$_2$ change the arsenene surface to p-type semiconductor resulting in the enhanced conductivity.[44]

3.5   Ge-doped arsenene

The electronic properties of arsenene are found to be sensitive to adsorption of NH$_3$ or NO$_2$ molecules. In order to increase the sensitivity, we have investigated effect of doping Ge to arsenene surface. The choice of Ge as dopant relies on its electron deficient nature compare to As atoms and can make the doping
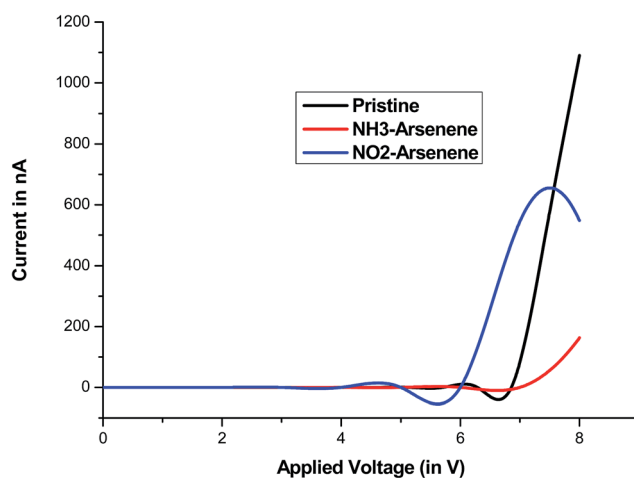

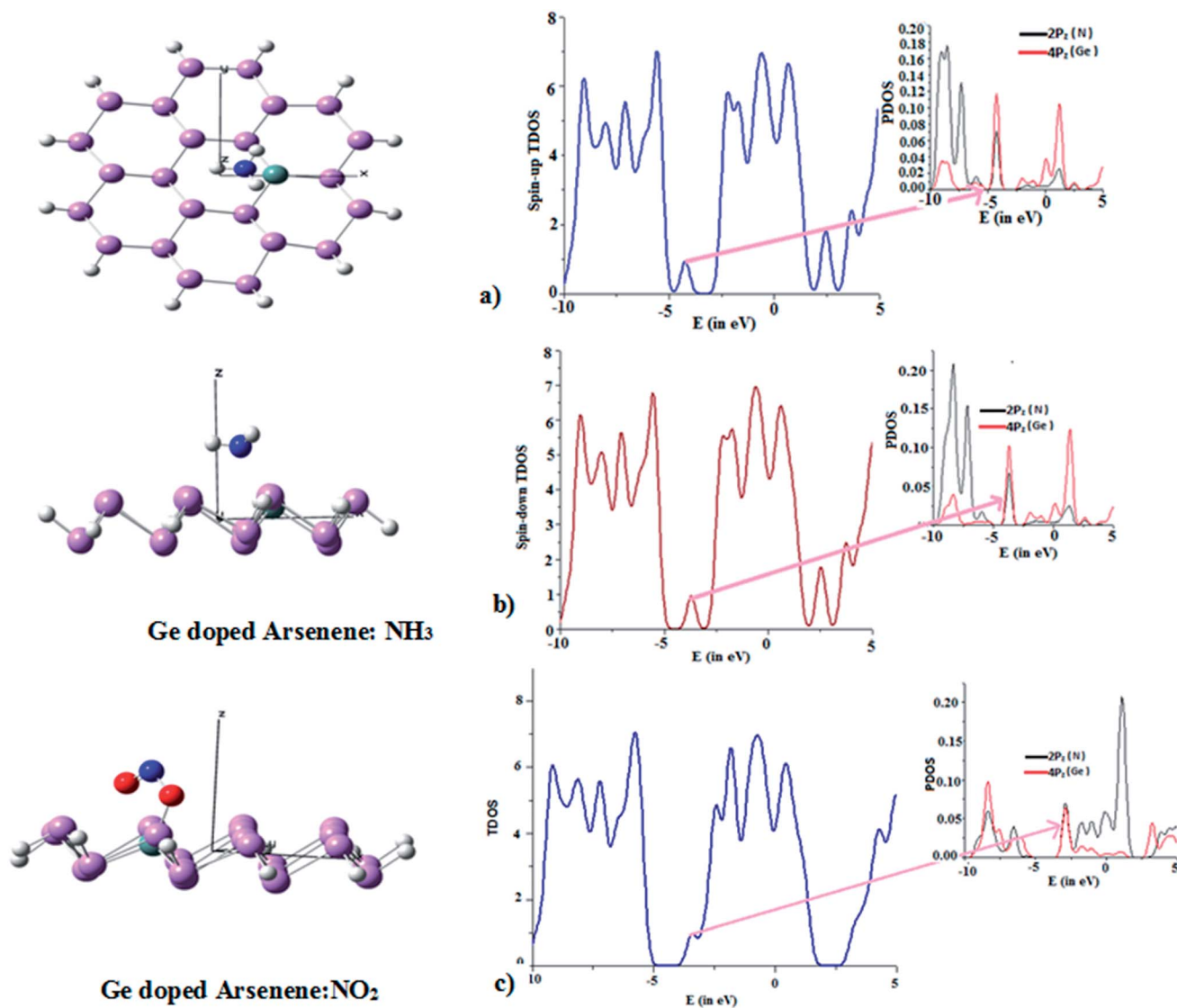Fig. 9 I–V relationship for pristine and NH$_3$/NO$_2$ exposed arsenene sheet.

Fig. 10 Optimized configuration and DOS of (a) NH_3 and (b) NO_2 adsorbed Ge doped arsenene.

sites chemically active. The following brief descriptions address Ge doping effect on NH_3/NO_2.

Fig. 10 shows the equilibrium configurations of NH_3 and NO_2 adsorbed on Ge-doped arsenene. The NBO analysis suggests NH_3 get intact to arsenene with a charge transfer of $0.22e$ in terms of natural atomic charges calculated in NBO analysis with a binding energy of -1.13 eV. As evident from Fig. 10a DOS analysis shows lone pair electrons localized at $2p_z$ orbital get depopulated by electronic charge transfer to $4p_z$ of Ge at HOMO of spin-up state. However for spin-down state calculations, the hybridization between these mentioned orbital fragments take place at LUMO (Fig. 10b). The binding energy for NO_2 is found to be -2.9 eV, with one of O atom gets bonded to Ge with bond length 1.98 Å. The strong binding between Ge and O can be attributed from the Ge–O bond length, which has electronic population of $1.96e$ and is consequence of strong electron dispersion on Ge from NO_2 also evident from Fig. 10c in terms of orbital hybridization.

4 Conclusions

In this work we performed theoretical analysis of newly proposed 2D monolayer of arsenene using DFT approach. Analysis suggests that proposed quasi 2D-sheet is stable and showing semiconducting behaviour. Where, NH_3 and NO_2 adsorbed at arsenene surface with significant binding energy of 0.87 eV and 0.81 eV, respectively, computed through G09 which very close to with ATK-VNL calculations. Mulliken and NBO charges suggest significant amount of electronic charge transfer in between gas molecules and arsenene. CDA, PDOS and molecular orbital diagram provide considerable evidence for binding of NH_3 and NO_2 at the quasi 2D-surface. The sensitivity of arsenene surface for NH_3 and NO_2 further have been analyzed in terms of I–V characteristic using NEGF method. The obtained result exhibits lowering of conductivity across the nanosheet surface on sensing NH_3. Contrary, NO_2 sensing made the sheet slightly more conductive in nature and is effect of electron

withdrawing nature of NO_2. Ge substituted on arsenene indicate strong adsorption of NH_3 and NO_2 molecule.

Acknowledgements

References

1 L. Li, Y. Yu, G. J. Ye, Q. Ge, X. Ou, H. Wu, D. Feng, X. H. Chen and Y. Zhang, *Nat. Nanotechnol.*, 2014, **9**, 372–377.

2 H. Liu, A. Neal, Z. Zhu, Z. Luo, X. Xu, D. Tomanek and P. D. Ye, *ACS Nano*, 2014, **8**, 4033–4041.

3 L. Kou, C. Chen and S. C. Smith, *J. Phys. Chem.*, 2015, **6**, 2794–2805.

4 Y. P. Wang, W. X. Ji, C. Zhang, S. Li, F. Li, P. Li, M. J. Ren, X. L Chen, M. Yuan and P. Wang, *Mater. Chem. Phys.*, 2016, **173**, 379–384.

5 W. Hu, N. Xia, X. Wu, Z. Li and J. Yang, *Phys. Chem. Chem. Phys.*, 2014, **16**, 6957–6962.

6 Y. P. Wang, C. W. Zhang, W. X Ji, R. W Zhang, P. Li, P. Wang, M. Ren, X. L. Chen and M. Yuan, *J. Phys. D: Appl. Phys.*, 2016, **49**, 055305.

7 Y. P. Wang, W. X. Ji, C. W. Zhang, P. Li, F. Li, M. Ren, X. Li Chen, M. Yuan and P. Wang, *Sci. Rep.*, 2016, **6**, 20342.

8 Y. P. Wang, W. X. Ji, C. W. Zhang, P. Li, F. Li, P. J. Wang, S. S. Li and S. S Yan, *Appl. Phys. Lett.*, 2016, **108**, 073104.

9 C. Kamal and M. Ezawa, *Phys. Rev. B: Condens. Matter Mater. Phys.*, 2015, **91**, 085423.

10 S. Zhang, Z. Yan, Y. Li, Z. Chen and H. Zeng, *Angew. Chem.*, 2015, **10**, 3112–3115.

11 Z. Zhang, J. Xie, D. Yang, Y. Wang, M. Si and D. Xue, *Appl. Phys. Express*, 2015, **8**, 055201.

12 A. Tyagi, V. Sharma and A. Srivastava, *Adv. Sci. Lett.*, 2014, **20**, 1570–1573.

13 A. Srivastava, C. Bhat, S. K. Jain, P. K. Mishra and R. Brajpuriya, *J. Mol. Model.*, 2015, **21**, 1–8.

14 A. Srivastava, V. Sharma, K. Kaur, M. S. Khan, R. Ahuja and V. K. Rao, *J. Mol. Model.*, 2015, **21**, 1–7.

15 M. S. Khan, A. Srivastava, R. Chauraiya, M. S. Khan and P. Dua, *Chem. Phys. Lett.*, 2015, **636**, 103–109.

16 A. Srivastava, M. S. Khan, S. K. Gupta and R. Pandey, *Appl. Surf. Sci.*, 2015, **356**, 881–887.

17 R. Chandiramouli, A. Srivastava and V. Nagarajan, *Appl. Surf. Sci.*, 2015, **351**, 662–672.

18 S. K. Jain and A. Srivastava, *Adv. Sci. Lett.*, 2014, **20**, 1624–1630.

19 B. Anand, M. Karakaya, G. Prakash, S. S. S. Sai, R. Philip, P. Ayala, A. K. Sood, A. Srivastava, A. Rao and R. Podila, *RSC Adv.*, 2015, **5**, 59556–59563.

20 G. Ko, H.-Y. Kim, J. Ahn, Y.-M. Park, K.-Y. Lee and J. Kim, *Curr. Appl. Phys.*, 2010, **10**, 1002–1004.

21 H. J. Yoon, D. H. Jun, J. H. Yang, Z. Zhou, S. S. Yang and M. M. Cheng, *Sens. Actuators, B*, 2011, **157**, 310–313.

22 M. Kharatha, A. Vaez, A. Seyed and H. Rozatian, *Mol. Phys.*, 2013, **111**, 3726–3732.

23 Y.-H. Zhang, Ya-B. Chen, K.-G. Zhou, C.-H. Liu, J. Zeng, H.-L. Zhang and Y. Peng, *Nanotechnology.*, 2009, **18**, 185504.

24 A. E. Reed, L. A. Curtiss and F. Weinhold, *Chem. Rev.*, 1988, **88**, 899–926.

25 M. J. Frisch, *et al.*, *Gaussian09, Revision A.02*, Gaussian, Inc., Wallingford CT, 2009.

26 http://www.quantumwise.com.

27 J. P. Perdrew, K. Burke and M. Ernzerhof, *Phys. Rev. Lett.*, 1997, **78**, 1396.

28 S. I. Gorelsky, *AOMix: Program for Molecular Orbital Analysis*, York University, Toronto, 1997.

29 S. I. Gorelsky and A. B. P. Lever, *Organomet. Chem.*, 2001, **635**, 187–196.

30 E. I. Solomon, S. I. Gorelsky and A. Dey, *J. Comput. Chem.*, 2006, **27**, 1415–1428.

31 W. Macyk, K. Szacilowski, G. Stochel, M. Buchalska, J. Kuncewicz and P. Labuz, *Coord. Chem. Rev.*, 2010, **254**, 2687–2701.

32 A. Srivastava, Md. S. Khan, S. K. Gupta and R. Pandey, *Appl. Surf. Sci.*, 2015, **356**, 881–887.

33 M. S. Khan and M. S. Khan, *Int. Nano Lett.*, 2012, **2**, 1–7.

34 M. S. Khan and M. S. Khan, *Phys. E*, 2012, **44**, 1857–1861.

35 N. Troullier and J. L. Martins, *Phys. Rev. B: Condens. Matter Mater. Phys.*, 1991, **43**, 1993.

36 M. Brandbyge, J. L. Mozos, P. Ordejon, J. Taylor and K. Stokbro, Density functional method for nonequilibrium electron transport, *Phys. Rev. B: Condens. Matter Mater. Phys.*, 2002, **65**, 165401.

37 S. Datta, *Quantum Transport: Atom to Transistor*, Cambridge University, Press, Cambridge, UK, 2005.

38 M. G. Silveirinha and N. Engheta, *Phys. Rev. B: Condens. Matter Mater. Phys.*, 2012, **86**, 161104.

39 H. Luth, *et al.*, *Surfaces and interfaces of solids*, Springer-Verlag, 1993, ISBN 978-3-540-56840-7.

40 S. I. Gorelsky and E. I. Solomon, *Theor. Chem. Acc.*, 2008, **129**, 57–65.

41 S. Dapprich and S. G. J. Frenking, *J. Phys. Chem.*, 1995, **99**, 9352–9362.

42 G. Frenking and N. Frohlich, *Chem. Rev.*, 2000, **100**, 717–774.

43 H. D. Cornean, A. Jensen and V. Moldoveanu, *J. Math. Phys.*, 2005, **46**, 042106.

44 H. Bai and G. Shi, *Sensor*, 2007, **7**, 267–307.